Optical manipulation and study of single gold nanoparticles in solution

Ruijgrok, P.V.

Cover Page

Universiteit Leiden

The handle http://hdl.handle.net/1887/18933 holds various files of this Leiden University dissertation.

Author: Ruijgrok, Paul Victor
Title: Optical manipulation and study of single gold nanoparticles in solution
Date: 2012-05-10

Appendices

A

Thermal and optical constants for selected materials

Table A.1: Thermal and optical constants for selected materials at room temperature and normal pressure [a]

Substance	n [b]	$10^4 \times \frac{\partial n}{\partial T}$ K^{-1}	$10^{-6} \times C_p$ $J\,m^{-3}\,K^{-1}$	κ $W\,m^{-1}\,K^{-1}$	$10^{10} \times \Sigma_{PT}$ $m^3\,J^{-1}$	$10^3 \times FOM$ $m\,W^{-1}$
BK7 glass	1.52	-0.13	2.2	1.1	0.09	0.02
PMMA	1.49	-1.2	1.4	0.2	1.3	0.90
Water	1.33	-0.9	4.2	0.56	0.29	0.21
Glycerol	1.47	-2.7	2.6	0.28	1.5	1.4
Ethanol	1.36	-4.4	1.9	0.17	3.1	3.5
Hexane	1.37	-5.5	1.5	0.12	5.0	6.1
Pentane	1.36	-6.0	1.5	0.14	5.6	6.0
Chloroform	1.45	-6.2	1.4	0.13	6.3	7.0
Carbon tetrachloride	1.47	-6.1	1.3	0.10	7.1	8.6
Carbon disulfide	1.63	-8.1	1.3	0.16	11	8.2

[a] The tabulated values for each substance are the refractive index n and its derivative with respect to temperature $\frac{\partial n}{\partial T}$, the heat capacity at constant pressure C_p, the thermal conductivity K, the photothermal strength $\Sigma_{PT} = n \left| \frac{\partial n}{\partial T} \right| \frac{1}{C_p}$, and the photothermal figure-of-merit $FOM = n \left| \frac{\partial n}{\partial T} \right| \frac{1}{K}$. Values are from the CRC Handbook of Chemistry and Physics (49th ed.) and Bialkowski.[94]

[b] For sodium light ($\lambda = 589.3$ nm), CRC Handbook of Chemistry and Physics

B

Optical microscope

objective mount

excitation objective

flow cell

collection objective

objective mount

filter/iris mount

optical axis

positioning ledge

support posts

Z translation stage

solid base

X/Y/Z piezo scanner

1D translation stage
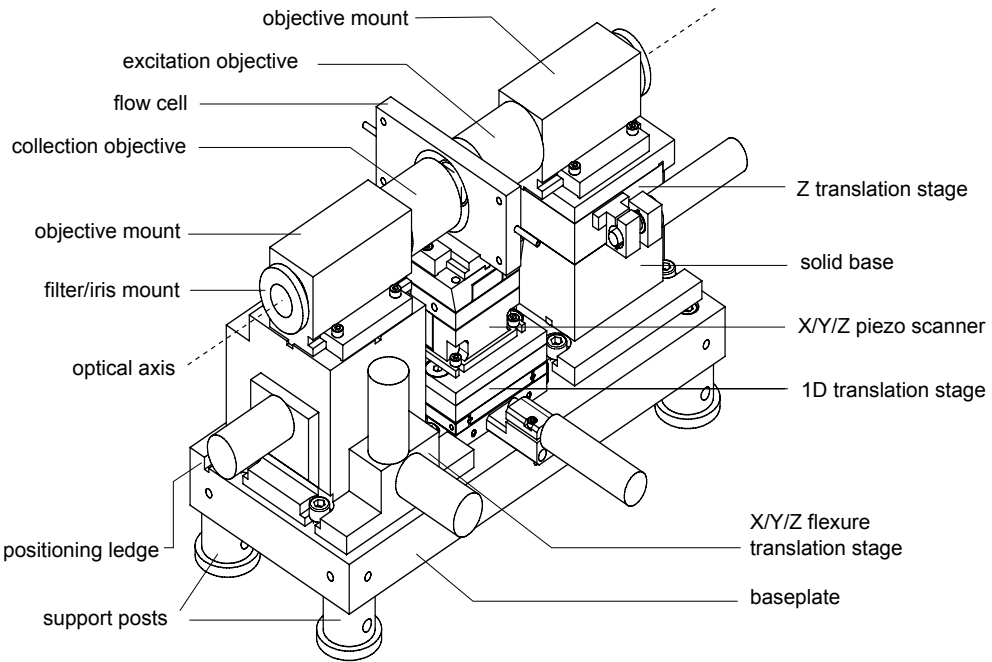
X/Y/Z flexure
translation stage

baseplate

Figure B.1: Optical microscope assembly constructed in this thesis, in a configuration as used in part of the reported experiments. Three independent constructions are mounted on a 25 mm thick aluminium baseplate, to support the excitation-objective, the sample holder/flow-cell and the collection-objective. The constructions can be removed and repositioned accurately with the help of positioning ledges. The design aims to achieve high mechanical stability and low thermal drift by a compact, stiff construction and a minimum number of translation elements. The optimization is directed to achieve the highest stability for the relative position between the excitation objective and the sample holder (flow-cell).
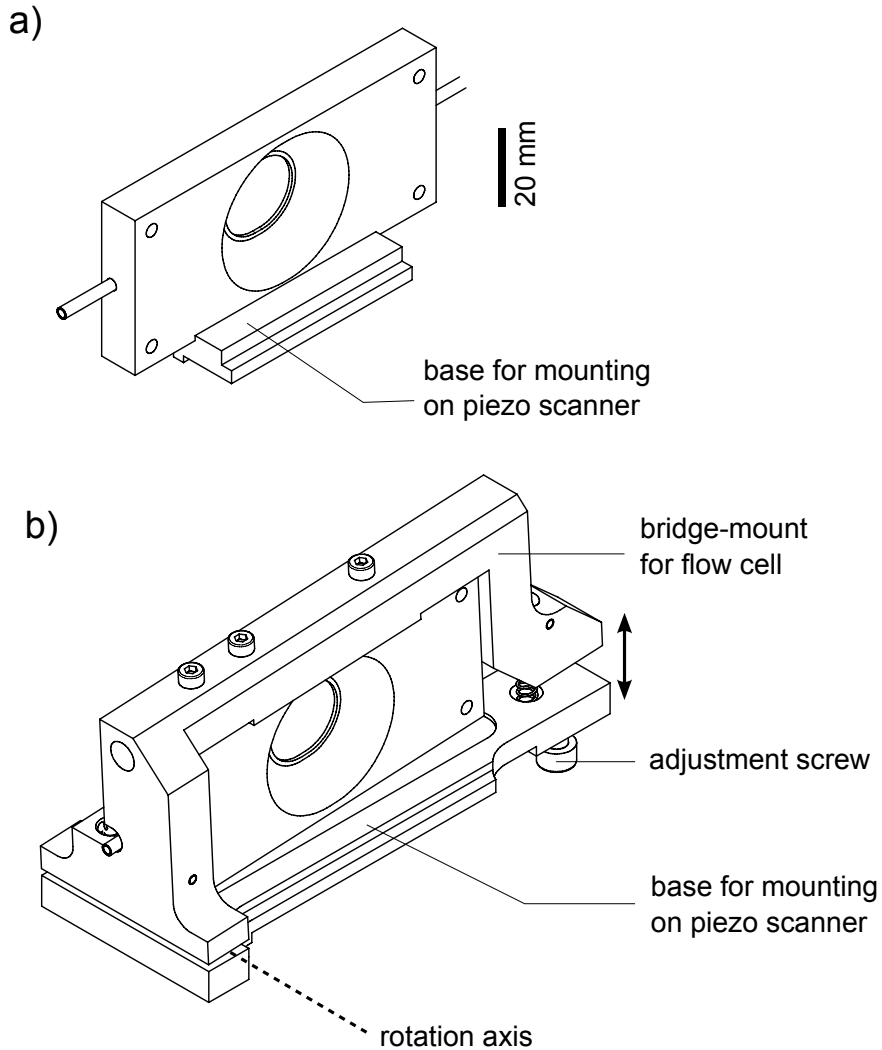
a)

20 mm

base for mounting
on piezo scanner

b)

bridge-mount
for flow cell

adjustment screw

base for mounting
on piezo scanner

rotation axis

Figure B.2: Two configurations to mount the flow-cell on the piezo-scanner in the microscope. a) Fixed mount. b) Mount that allows manual translation in the vertical direction, while maintaining mechanical stability. The flow-cell is mounted hanging on a spring-loaded bridge construction, that can be rotated around an axis (two ball joints) on one end with an adjustment screw on the other end. At the center of the flow cell, the rotation amounts to an effective vertical translation, over a range up to ± 1 mm. This movement facilitates the search for a specific location on the sample over a region larger than the $100\,\mu$m range of the piezo-scanner. The experiments reported in this thesis were performed with the fixed mount.

a)

top coverslip

inlet

PDMS

channel

bottom coverslip
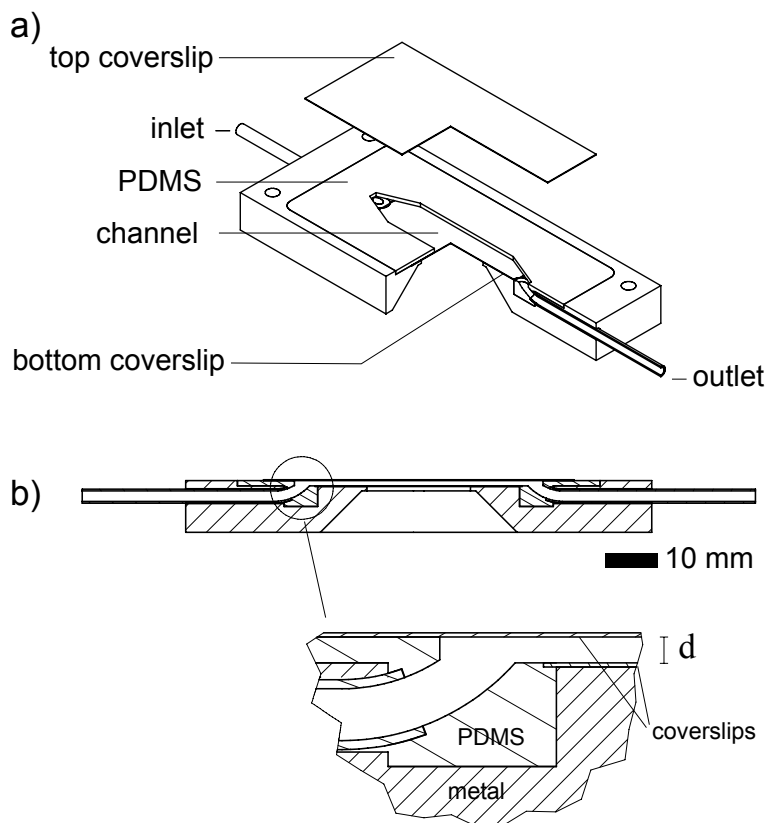
outlet

b)

10 mm

d

PDMS

coverslips

metal

Figure B.3: Details of the flow-cell used in the experiments reported in this thesis. a) Perspective view. The construction with the flexible in/outlets and the bottom coverslip embedded in polydimethylsiloxane (PDMS) can be remade repeatedly, when desired. A micro-fluidic channel is cut out from the PDMS layer by hand. The top coverslip forms the closure of the micro-fluidic channel when pressed on the PMDS, and can be repeatedly re-applied. b) Side view. The inset shows a detailed view of the connection between the inlet of the cell and the micro-fluidic channel. The design eliminates contact of the fluid with the metal part of the flow-cell casing. Channel thickness *d* could be varied between 40 μm and 1 mm by the use of metal casings with different chamber depths. The design was based on a design from the group of Dr. J. van Noort (Leiden University).

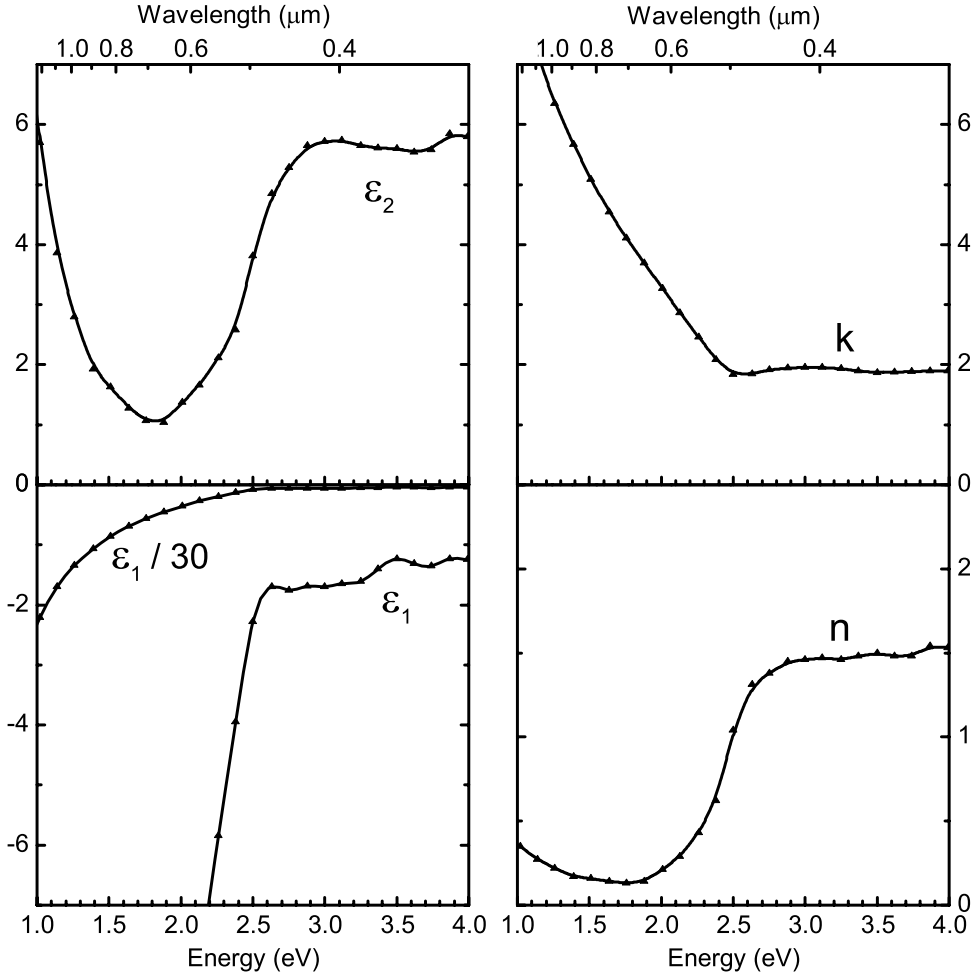# C

Optical constants of bulk gold

Figure C.1: The optical constants of bulk gold at room temperature as a function of photon energy, used throughout this thesis. The data are from Johnson and Christy[113] and were obtained from reflection and transmission measurements on vacuum-evaporated thin films of gold. The individual panels display the real and imaginary parts of the complex dielectric function $\tilde{\epsilon} = \epsilon_1 + i\epsilon_2$ and the real and imaginary parts of the complex refractive index $\tilde{n} = n + ik$. The complex dielectric function and the complex refractive index are related as $\tilde{\epsilon} = \tilde{n}^2$, so that $\epsilon_1 = n^2 - k^2$ and $\epsilon_2 = 2nk$. The symbols represent tabulated measured values, while the solid lines are spline interpolations.

D

Hydrodynamic friction coefficients

As the friction coefficients for the gold nanorod we have used the analytical expressions derived by Francis Perrin for a prolate spheroid[127] with aspect ratio ρ. The friction coefficient ξ_r for rotation around a short principal axis is given as

$$\xi_r = 8\eta V \frac{\rho^4 - 1}{(2\rho^2 - 1)S(\rho) - 2\rho^2} \tag{D.1}$$

where η is the medium's viscosity, V is the hydrodynamic volume, and

$$S(\rho) = \frac{2\rho}{\sqrt{\rho^2 - 1}} \log\left\{\rho + \sqrt{\rho^2 - 1}\right\}. \tag{D.2}$$

For translation, the friction coefficients are given by

$$\xi_{tr,\parallel} = 16\pi\eta \left(\frac{3\rho^2 V}{4\pi}\right)^{1/3} \frac{\rho^2 - 1}{(2\rho^2 - 1)S(\rho) - 2\rho^2} \tag{D.3}$$

for translation parallel to the long axis of the spheroid, and

$$\xi_{tr,\perp} = 32\pi\eta \left(\frac{3\rho^2 V}{4\pi}\right)^{1/3} \frac{\rho^2 - 1}{(2\rho^2 - 3)S(\rho) + 2\rho^2} \tag{D.4}$$

for translation perpendicular to the long axis of the spheroid.

The friction coefficients for translation and rotation are plotted as functions of aspect ratio in Fig. D.1(a) and Fig. D.1(b) respectively, for an ellipsoid
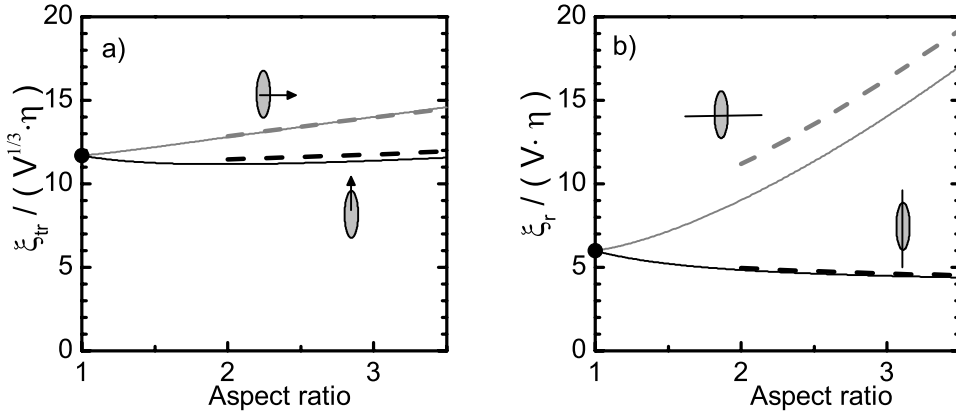
Figure D.1: Hydrodynamic friction coefficients for ellipsoids, cylinder and spheres. a) Translational friction coefficients as functions of aspect ratio for a prolate spheroid (solid lines[127]) and a cylinder (dashed lines[217]) of the same volume V. Black (Grey) curves: friction coefficients for translation parallel (perpendicular) to the symmetry axis of the rod. The Stokes equation $\xi_{tr} = 6\pi\eta \left(3V/(4\pi)\right)^{1/3}$ is shown as a limit for an aspect ratio of 1 (black dot). b) Rotational friction coefficients as functions of aspect ratio for a prolate spheroid (solid lines[127]) and a cylinder (dashed lines[129,217]) of the same volume V. Black (Grey) curves: friction coefficients for rotation around the long symmetry axis (one of the short symmetry axes) of the rod. The Stokes equation $\xi_r = 6\eta V$ is shown as a limit for an aspect ratio of 1 (black dot).

of constant volume. As the real shape of our gold nanorods is not an ellipsoid, but something close to a spherically capped cylinder, the expressions for ellipsoids are expected to provide an approximate value only. For comparison, we also plot the values of the friction coefficients for cylinders, as calculated by Tirado et al.[217] Whereas the expression for the friction coefficients for spheroids are valid for particles of arbitrary aspect ratio, the expressions for cylinders are expected to provide reliable results only for aspect ratios larger than 2.

Temperature-dependent viscosity of water

As can be seen in Fig. D.2, the temperature dependence of the viscosity of water is well described by a Vogel-Fulcher law as:[90]

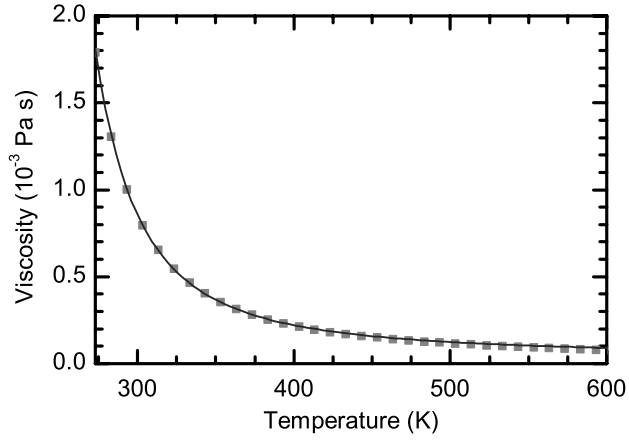$$\eta(T) = \eta_\infty \exp\left(\frac{A}{T - T_{VF}}\right), \tag{D.5}$$

Figure D.2: Viscosity of water as function of temperature, at vapor saturation pressure. The influence of pressure on viscosity in this range is small. Squares: data derived from NIST Chemistry Webbook.[218] Solid line: Vogel-Fulcher law with parameters as used in this study.

with $\eta_\infty = 0.0298376\,10^{-3}$ Pa $\cdot$ s, $A = 496.889$ K and $T_{\mathrm{VF}} = 152.0$ K.

E

Calculation of the orientational trap stiffness from a measured spectral intensity ratio

We calculate the rotational trap stiffness κ_r from the time averaged spectral intensity ratio $\langle I_\parallel \rangle_t / \langle I_\perp \rangle_t$. Here $\langle I_\parallel \rangle_t$ and $\langle I_\perp \rangle_t$ are the time-averaged values of the intensity of the longitudinal plasmon resonance, detected with analyzer parallel and perpendicular to the trap laser polarization, respectively. The incoming light is white light from a Xenon arc lamp, therefore it is unpolarized (randomly polarized) thermal light. We assume ergodicity and evaluate the intensity ratio as

$$\frac{\langle I_\parallel \rangle_t}{\langle I_\perp \rangle_t} = \frac{\langle \cos^2 \theta \rangle_T}{\langle \sin^2 \theta \cos^2 \phi \rangle_T} \tag{E.1}$$

where θ and ϕ are polar angles of the rod axis with respect to the trap polarization, as defined in Fig. E.1 a), and the subscripted T denotes a thermally weighted averaging. The weights in the averaging are given by the Boltzmann distribution $\propto \exp\left\{ -U(\theta)/k_B \widetilde{T_B} \right\}$ where the potential is $U(\theta) = -\frac{1}{2} \kappa_r \cos^2 \theta$. We find for the numerator[219]

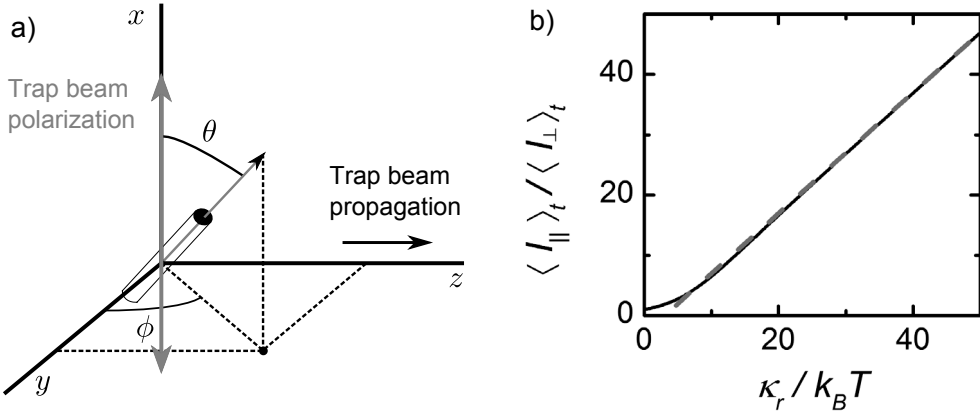$$\langle \cos^2(\theta) \rangle = \frac{1}{2\sqrt{\Xi} \mathrm{Daw}(\sqrt{\Xi})} - \frac{1}{2\Xi} \tag{E.2}$$

Figure E.1: a) Coordinate system. b) Calculated spectral intensity ratio $\langle I_\parallel \rangle_t / \langle I_\perp \rangle_t$ versus rotational trap stiffness κ_r. Solid line: analytical solution (eq. E.6). Dashed line: Linear approximation for high trap stiffness (eq. E.7).

where we have used the Dawson function defined as

$$\mathrm{Daw}(z) \equiv \exp(-z^2) \int_0^z dt \exp(t^2) \tag{E.3}$$

and

$$\Xi \equiv \frac{\kappa_r}{2k_B \widetilde{T_B}} \tag{E.4}$$

Noting that the angles ϕ and θ are independent, and that there is no preferred value for the angle ϕ we find for the denominator

$$\langle \sin^2(\theta) \cos^2(\phi) \rangle = \frac{1}{2} \left(1 - \langle \cos^2(\theta) \rangle \right) \tag{E.5}$$

and we evaluate the intensity ratio as

$$\langle I_\parallel \rangle_t / \langle I_\perp \rangle_t = \frac{2\sqrt{\Xi} - 2\mathrm{Daw}(\sqrt{\Xi})}{2\Xi\mathrm{Daw}(\sqrt{\Xi}) - \sqrt{\Xi} + \mathrm{Daw}(\sqrt{\Xi})} \tag{E.6}$$

The relation is plotted in Fig. E.1 b). For $\kappa_r \gg k_B \widetilde{T_B}$, the function is well approximated by the first terms in the power series expansion:

$$\langle I_\parallel \rangle_t / \langle I_\perp \rangle_t \simeq \frac{\kappa_r}{k_B \widetilde{T_B}} - 3 \tag{E.7}$$

which is shown as the dotted line in Fig. E.1 b).

F

Correlation functions in a potential

In this appendix we discuss the calculation of the autocorrelation functions of light scattered by a trapped nanoparticle.

The goal is to evaluate the autocorrelation function of the scattered intensity I, defined as

$$G^{(2)}(\tau) = \frac{\langle I(t)I(t+\tau)\rangle_t}{\langle I(t)\rangle_t^2} \tag{F.1}$$

where $I(t)$ is the scattered intensity at a time t and $I(t+\tau)$ is the scattered intensity a time τ later. The intensity is assumed to be a stationary random function of time (we take $t = 0$ in the following).

We make the assumption that the rotational and translational motions of the trapped particle are independent[1], so that we can write

$$G^{(2)}(\tau) = G^{(2)}_{tr}(\tau)G^{(2)}_r(\tau) \tag{F.2}$$

where $G^{(2)}_{tr}(\tau)$ and $G^{(2)}_r(\tau)$ are the translational and rotational factors of the correlation function, respectively.

---

[1]This is not strictly true for the gold nanorod in the trap. Indeed, both the translational friction and translational trap-stiffness depend on the orientation of the rod. The rotational stiffness is proportional to the local intensity, and thus depends on the position of the rod in the trap.

Rotational autocorrelation function

We outline the calculation of the rotational part of the autocorrelation function of light scattered by the rod in the optical trap, for the case where the incoming excitation light is linearly polarized parallel to the trap laser, and the scattered light is collected behind an analyzer perpendicular to the trap laser polarization. In the particular detection geometry considered here, the scattered intensity is related to the orientation of the rod as

$$I \propto \cos^2\theta \sin^2\theta \cos^2\phi \qquad (F.3)$$

where θ and ϕ are polar angles of the rod axis with respect to the trap polarization, as defined in Fig. E.1 a). We have assumed the scattering by the transverse plasmon resonance to be negligible, and the absence of any background intensity.

The orientational dynamics of the rod in the optical potential are governed by the Fokker-Planck equation,[220–222] which relates the probability distribution of orientation of the rod $p(\theta,\phi,t)$ to the rotational friction coefficient ξ_r for rotation around a short principal axis, and the potential $U(\theta) = -1/2\kappa_r \cos^2\theta$ as

$$\frac{\partial p}{\partial t} = \frac{1}{\xi_r}\left[k_B T \nabla_S^2 p + \nabla_S \cdot (p\nabla_S U)\right] \qquad (F.4)$$

where ∇_S denotes the gradient operator restricted to the surface of a sphere with radius 1.

To proceed with the calculation, we assume ergodicity to replace the time average $\langle...\rangle_t$ in the correlation function by the thermally weighted ensemble average $\langle...\rangle_T$. The expressions for $I(0)$ and $I(\tau)$ can be formulated in terms of the probability $p(\theta_0,\phi_0,0)$ to find the rod at an orientation (θ_0,ϕ_0) at time 0 (we take this to be the Boltzmann distribution) and the conditional probability $p(\theta,\phi,\tau|\theta_0,\phi_0,0)$ to find the rod at an orientation (θ,ϕ) at time τ given that it was at an orientation (θ_0,ϕ_0) at time 0.

An analytic solution for $p(\theta,\phi,\tau|\theta_0,\phi_0,0)$ can be found in the limit of high rotational trap stiffness. When $\kappa_r \gg k_B T$, the angular deviations of the rod from the orientation parallel to the trap laser polarization will be small: $\theta \ll 1$. The problem then becomes that of a thermally excited harmonic oscillator. The potential is $U(\theta) = \frac{1}{2}\kappa_r\theta^2 + \text{constants}$, and we consider the expression for the thermal average with terms up to third order in θ. In addition, the evaluation of integrals for the thermal averaging can be simplified by extending the integration limits from $\theta \in [0,2\pi)$ to $\theta \in [0,\infty)$ as the probability

for the occupation of large angles is negligible. To simplify the calculation, and allowed because we have assumed to the excursions from equilibrium to be small, we change from 2D polar to 2D Cartesian coordinates $\chi = \theta \cos \phi$ and $\Psi = \theta \sin \phi$. The required solution to the Fokker-Planck equation is:[220]

$$p(\chi, t | \chi_0, t_0) = \sqrt{\frac{\kappa_r}{2\pi k_B T S(\tau, 0)}} \exp \left[-\frac{\kappa_r \left(\chi - \chi_0 e^{-(t-t_0)/(2\tau_r)} \right)^2}{2 k_B T S(t, t_0)} \right] \tag{F.5}$$

with

$$\tau_r = \frac{\xi_r}{2\kappa_r} \tag{F.6}$$

and

$$S(t, t_0) = 1 - e^{-(t-t_0)/\tau_r} \tag{F.7}$$

Evaluating the expression for the correlation function with these approximations, we find

$$G_r^{(2)}(\tau) = 1 + 2 \exp(-\tau/\tau_r) \tag{F.8}$$

where

$$\tau_r = \frac{\xi_r}{2\kappa_r} \tag{F.9}$$

It is interesting to compare the rotational correlation times as discussed here for a gold nanorod in an optical potential to correlation times measured on ensembles of gold nanorods, both freely diffusing[80,133] and weakly trapped.[80] In the case of freely diffusing nanorods the correlation times are determined by the inverse of the rotational diffusion constant D_r, itself the ratio of the thermal energy $k_B T$ to the rotational friction coefficient ξ_r. Specifically, the rotational contrast observed in a configuration with vertically polarized excitation light and horizontally polarized detection decays with a time constant $\tau_{r,\text{free}} = 1/12 D_r = \xi_r/(12 k_B T)$.[133]

As the orientational trap stiffness κ_r can reach values significantly exceeding $6\,k_B T$ (we demonstrate an orientational trap stiffness up to $40\,k_B T$ in this thesis), the rotational correlation times observed on a gold nanorod in an optical trap can be significantly shorter than rotation times for freely diffusing rods. In addition, correlation times in a trap will be shorter due to the heating of the rods: the effective viscosity for the rotation of the hot rod can be significantly below the viscosity of the medium at room temperature.

Translation autocorrelation function

The calculation of the translational part of the autocorrelation function follows along the same line as the calculation of the rotational part. For the translational motion, the relevant intensity function is a Gaussian beam

$$I(x,y,z) \propto \exp\left\{ -2\left(\frac{x^2}{w_x^2} + \frac{y^2}{w_y^2} + \frac{z^2}{w_z^2} \right) \right\} \tag{F.10}$$

with widths w_x, w_y, w_z in x, y and z directions respectively.

In each dimension, the potential for a trapped particle is harmonic, for example in the x-direction given by $U = \frac{1}{2}\kappa_{tr,x}x^2$, with $\kappa_{tr,x}$ the relevant translational friction coefficient. We assume that the motions in the three dimensions are independent, so that the correlation function is simply a product over the functions in the one-dimensional case.

As for the rotational case, the translational dynamics of the trapped partial are governed by the Fokker-Planck equation (as in F.4, with now the translational friction coefficient, and the gradient operator ∇). Because the potential for translations is harmonic, as approximated for the rotational case, the solution of the Fokker-Planck equation is as in Eq. F.5, now with

$$\tau_{tr} = \frac{\zeta_{tr}}{2\kappa_{tr}} \tag{F.11}$$

Evaluating the expression for the correlation function we find, for each dimension,

$$G_{tr}^{(2)}(\tau) = \sqrt{\frac{A+1}{A+(1-\exp(-\tau/\tau_{tr}))}} \tag{F.12}$$

where

$$A = \frac{1}{4}\left(\frac{\kappa_{tr}w^2}{2k_BT} \right)^2 + \frac{\kappa_{tr}w^2}{2k_BT} \tag{F.13}$$

with w the width of the Gaussian beam in the evaluated dimension and

$$\tau_{tr} = \frac{\zeta_{tr}}{2\kappa_{tr}} \tag{F.14}$$

For a stiff trap, the translational fluctuations are much smaller than the focus size w, and we have $\kappa_{tr}w^2/(2k_BT) \gg 1$. In this case we can approximate Eq. F.12 in each dimension by a Taylor expansion in $1/A$ as

$$G_{tr}^{(2)} \approx 1 + \frac{1}{2A}\exp\left(-\tau/\tau_{tr}\right) \tag{F.15}$$

G

Heat dissipation of metal spheres and ellipsoids in water

We examine the difference between the steady-state temperature profiles a-round a heated metal sphere and an prolate spheroid with a moderate aspect ratio (less than 5), for particles dissipating a power P_{diss} in a medium with a thermal conductivity K_m (independent of temperature). We take the approximation that the heat conductivity of the metal is infinite, therefore that the temperature in the particle is uniform. Within these approximations, the steady-state heat diffusion equation is a Poisson-type equation[223]

$$\nabla^2 T = -\frac{\dot{q}}{K_m} \tag{G.1}$$

where $\dot{q}$ is the volumetric heat release rate and K the thermal conductivity of the medium. Following the analogy with the equation for an electrostatic potential, the solution of Poisson's equation for heat conductivity in steady state for a prolate spheroidal source is[224]

$$\Delta T(\xi) = \frac{1}{8\pi K_m} \frac{P_{\text{diss}}}{\sqrt{a^2 - b^2}} \log\left(\frac{\sqrt{\xi + a^2} + \sqrt{a^2 - b^2}}{\sqrt{\xi + a^2} - \sqrt{a^2 - b^2}}\right) \tag{G.2}$$

with a and b the major and minor semi-axis of the spheroid respectively, and ξ an ellipsoidal coordinate given by

$$\xi = \frac{1}{2}\left\{(x^2 + y^2 + z^2) - (a^2 + b^2)\right\}$$
$$+ \frac{1}{2}\sqrt{(a^2 + b^2)^2 + (x^2 + y^2 + z^2)^2 - 2x^2(b^2 - a^2) - 2(y^2 + z^2)(a^2 - b^2)}$$

(G.3)

The surface temperature of the particle is found for $\xi = 0$.

The analytical solution for the temperature change of the ellipsoid compared to that of the sphere with the same volume is shown in Fig. G.1. For an aspect ratio of 2, the temperature change is less than 5 %. This means that, to this degree of accuracy, we can replace the nanorod by a sphere with the same volume. The temperature profile around an ellipsoidal particle is presented in Fig. G.2.
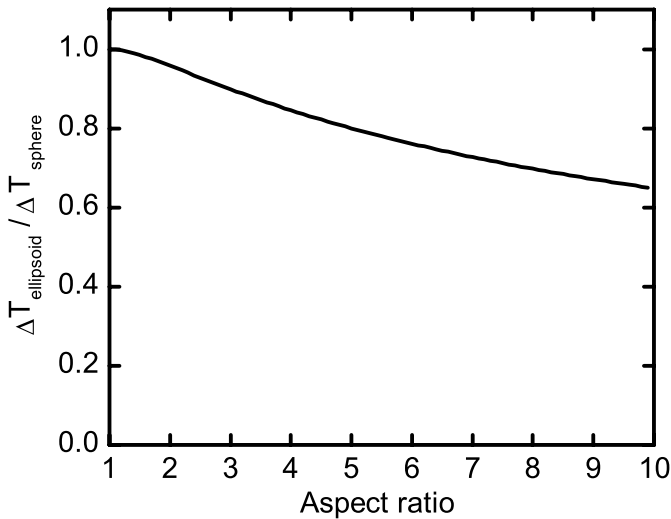

Figure G.1: Heat loss of an ellipsoid of revolution, relative to a sphere of the same volume, for a given dissipative power.

The change of thermal conductivity conductivity is less than a few percent in the whole temperature range of our experiments.[218] We therefore took the conductivity of water at room temperature in all our calculations.

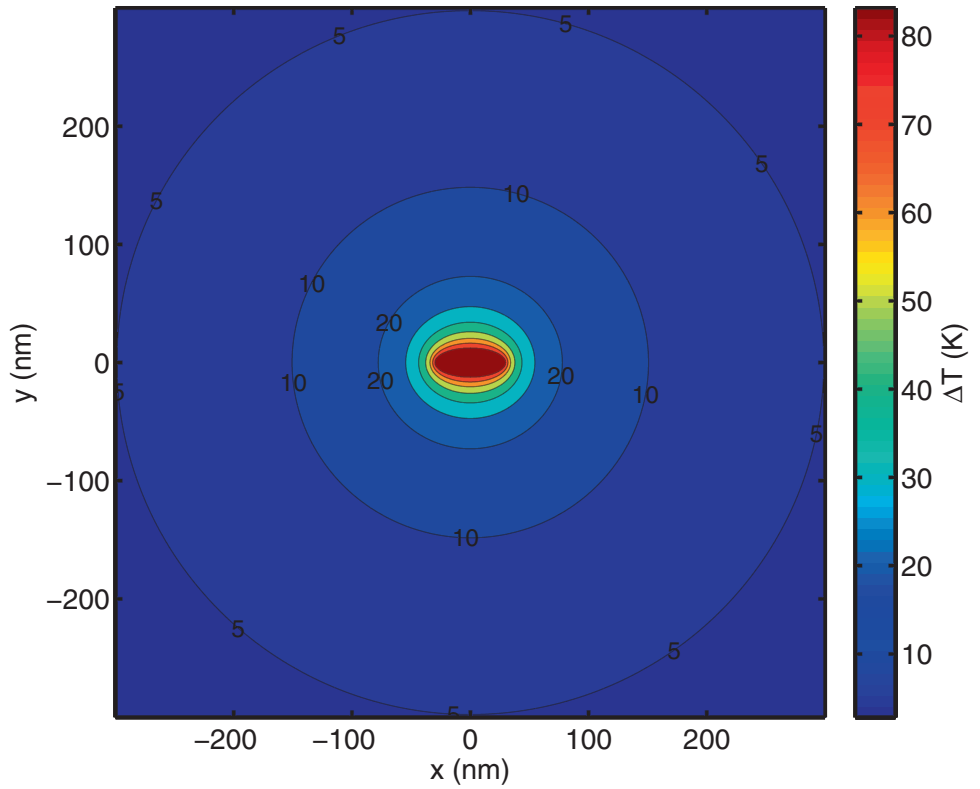**Figure G.2:** Distribution of temperature around an ellipsoidal gold nanoparticle in water, 25x60 nm. Intensity $2.385 \cdot 10^{11} \, \mathrm{W/m^2}$, $\sigma_{\mathrm{abs}} = 4.398 \cdot 10^{-17} \mathrm{m^2}$, $\Delta T_p = 83 \, \mathrm{K}$
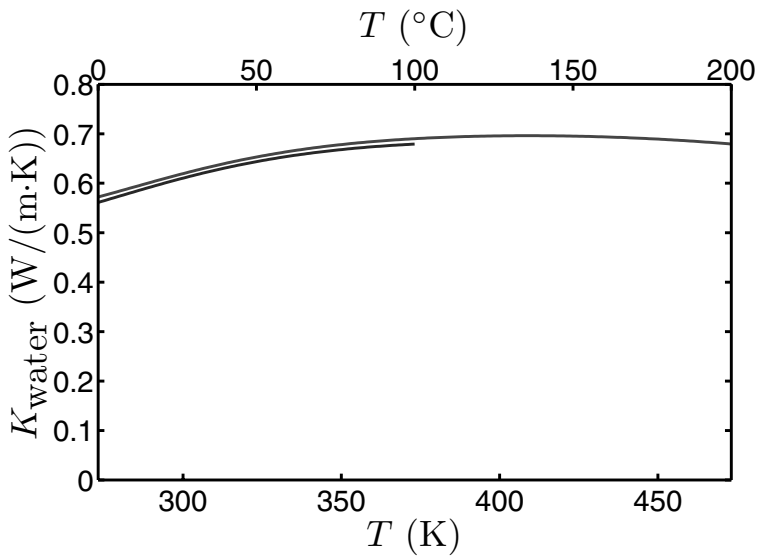
Figure G.3: Thermal conductivity of water as function of temperature, at 1 Atm. (bottom curve) and 200 Atm. (top curve). Data from NIST Chemistry Webbook.[218]

H

Model of temperature dependent dynamics in the optical trap

In this appendix we provide an overview of the model of the temperature dependent dynamics of gold nanorods in the optical trap as presented in Chapter 4, and discuss the assumptions made. We apply the model to measurements on three individual nanorods, the nanorod from Figure 4.3 in Chapter 4, as well as two additional rods.

Assumptions in the model

The model used to fit all experimental data in Chapter 4 in a consistent way involves a fair number of assumptions. The most important ones are listed hereafter.

1. **Point-spread-function of the trap intensity** – As discussed in Chapter 3, the local intensity in the trap was consistent with an effective numerical aperture $NA = 1.0$. We took the intensity at the focus of a Gaussian beam with this NA to calculate the local intensity acting on the rod, neglecting the shift along the axis and further aberrations of the beam.

2. **Absorption cross-section of rod** – This was calculated in the dipole approximation for an ellipsoid. This neglects shape deviations of the

actual rod, which, to a good approximation, is a cylinder capped with two hemispheres. Moreover, we tuned the ellipsoid's aspect ratio to match the longitudinal plasmon frequency found in the experiment. In addition, we introduced corrections for spontaneous emission, and for electron scattering at the rod's surfaces. With this model, we found a good agreement of the spectrum, including the width. This broadening of the plasmon may be induced by temperature, or by thiol-PEG groups. The absorption cross-section found in this model was 30%-50% too large to account for the observed temperature rise.

3. **Radiation pressure** – The weak absorption of trap photons by the nanorod gives rise to a recoil force that shifts the nanorod from the trap's center by some 200-300 nm. This effect was neglected in the calculation of the local intensity and of the restoring forces, as well as any photophoretic effect caused by an inhomogeneous temperature profile within the nanorod.

4. **Friction coefficients** – The translational and rotational damping of the rod was calculated with Perrin's formulas[225] for an ellipsoid, not for the cylindrical shape of the rod.

5. **Heat conduction around the rod** – We neglected the variation of the heat conductivity of water with temperature. Furthermore, we also neglected the effect of the PEG capping on heat conduction.

6. **Hot Brownian motion** – The effective viscosity for translation motion in the trap was taken as the one for free translational diffusion calculated by Rings et al.[90] This is a good approximation because the translational movement in the trap is slow, of the order of $100\,\mu$s.

7. **Effective rotational viscosity** – To fit the measured dependence of rotational times on translational times (see Fig. 3 in the main text), we had to introduce an effective viscosity for rotation which was lower than the previous one for translation. Whereas this viscosity cannot be smaller than the viscosity of water at the temperature of the nanorod, we found that this minimum viscosity reproduces well the measured vibrational damping. Therefore, we kept this effective viscosity without further justification.

8. **Polarization inhomogeneity in the focus** – Although the trap light at the center of the focus is linearly polarized in the focal plane along the

polarization of the trap laser, the polarization state seen by the nanorod changes when it moves around. We have neglected all depolarization effects induced by the motion of the nanorod, assuming the position of the rod to be very close to the focus. The deviation from linear polarization of the trap light will induce slight orientational deviations of the rod, which do not follow Boltzmann's statistics. However, the correlation time of these fluctuations should be that of the translational diffusion, much longer than that of the rotational diffusion. Such orientational effects were not considered in the analysis of the translational correlation. Similarly, deviations from the center of the trap give rise to depolarization of the scattered light which was neglected.

9. **Gold heating** – The temperature change in the trap leads to a change of the optical response of gold. According to the literature,[123] this effect is small and was neglected.

10. **Polymer conformational changes** – All effects related to the temperature dependence of the polymer brush on the nanoparticles have been neglected. The only effect of the polymer we consider is the introduction of a temperature-independent change of hydrodynamic volume compared to that of the bare nanorod.

Trap characteristics for three nanorods

Here we discuss the results of the combined measurement of the spectral intensity ratio and the correlation times on a single particle. We performed the measurements on a set of three individual nanorods from the same sample under identical parameters of the optical trap. The nanorods have slightly different aspect ratios, as we can conclude from the measured scattering spectra with resonances at 617 nm, 624 nm and 636nm.

The results are shown in Fig. H.1, with the same series of measurements on each rod organized in vertical columns. The measurements in the first column are on the same nanorod as in Fig. 1 of Chapter 4, the second and third column display the results on two additional rods. Row (a-f-k) displays the measured spectral intensity ratios. The rotational trap stiffness κ_r deduced from this ratio using eq. E.6 is shown in row (b-g-l). The bottom three rows display the measured rotation and translation correlation times, and their ratio. All three nanorods display qualitatively the same behavior.
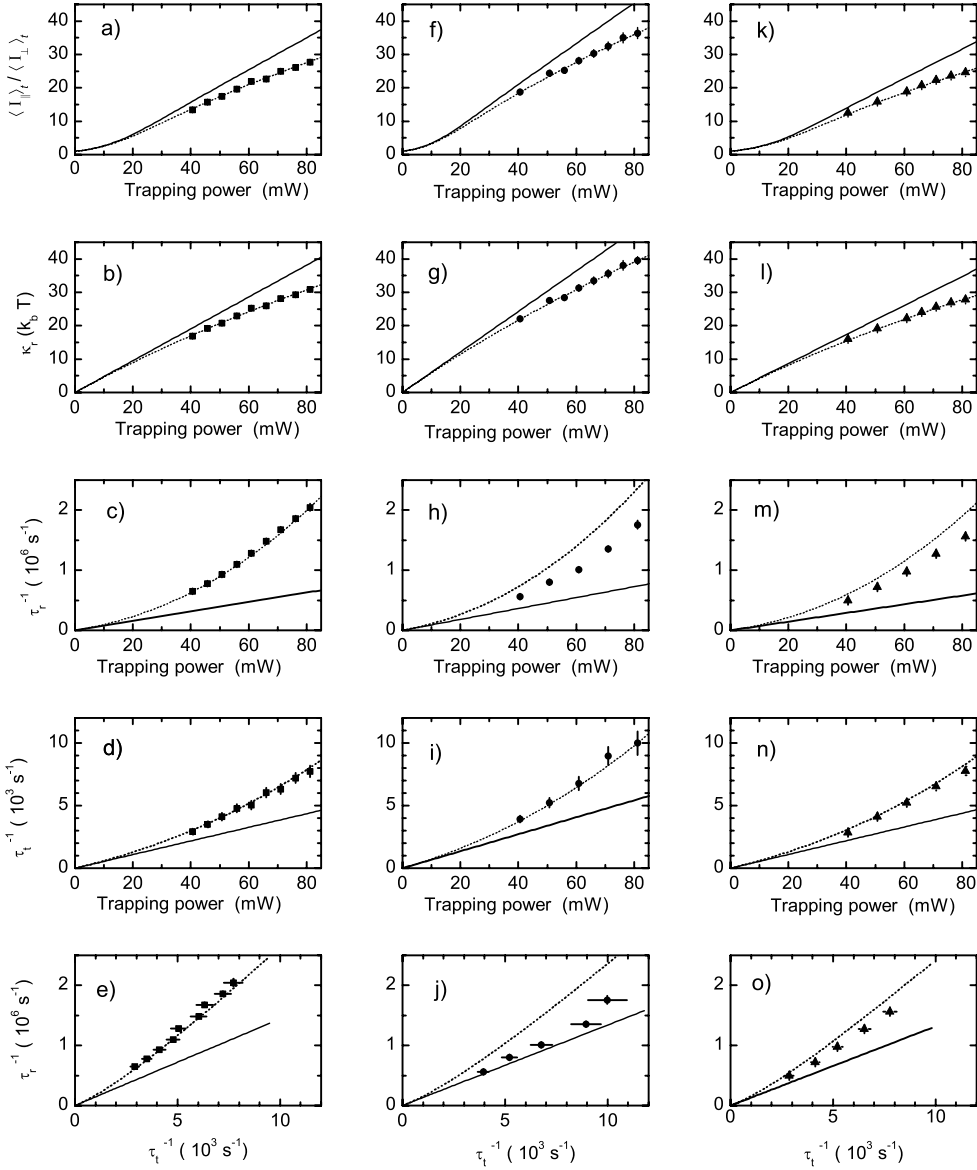
Figure H.1: Trap characteristics as functions of trapping power, for 3 individual gold nanorods, with resonance wavelength 624 nm (Column a-e, rod 1, the nanorod from Chapter 4), 636 nm (Column f-j, rod 2) and 617 nm (Column k-o, rod 3). See text for further details.

λ_L (nm)	κ_r ($k_B \widetilde{T}_B$)	V_p (10^4 nm^3)	κ_t (10^{-6} pN nm^{-1} mW^{-1})	ΔT_p (K mW^{-1})
624 ± 1	30.9 ± 0.6	2.1 ± 0.1	8.8 ± 0.5	0.89 ± 0.1
636 ± 1	39.5 ± 1.0	2.5 ± 0.1	11.7 ± 1.0	0.89 ± 0.1
617 ± 1	27.8 ± 1.0	2.2 ± 0.1	8.8 ± 0.5	0.93 ± 0.1

Table H.1: Trapping parameters for the three nanorods of Fig. H.1. The wavelength of the longitudinal plasmon resonance λ_L is determined experimentally. The rotational trap stiffness κ_r is directly computed from the experimentally measured spectral intensity ratio $\langle I_\parallel \rangle_t / \langle I_\perp \rangle_t$ via equation E.6. The values for the particle volume V_p and the transverse trap stiffness κ_t are determined from the fitting procedure. The value of the intensity at the trap focus at an incident trapping power of 80 mW was taken for all three particles as $I_0 = 2.12 \cdot 10^{11}$ W/m^2. The hydrodynamic thickness of the PEG capping layer of the gold nanorods was fitted to 5 nm.

Overview of the fitting procedure

The vertical display sequence of the measurements in Fig. H.1 follows the procedure that was used to make a global fit of our model with an effective temperature $\widetilde{T}_B$ and two effective viscosities η_r and η_t. In the model, the fitting parameters are the individual volumes of the three nanorods, the intensity of the trap laser, the effective hydrodynamic thickness of the capping layer of the rods and the transverse trap stiffness. For a given incident trap power, the measurements were fitted with a single intensity at the trap focus for all three particles. The hydrodynamic thickness of the capping layer was also kept the same for all three particles, independent of trapping power. The parameters determined from the fit are summarized in Table H.1.

Here we outline the sequence of steps in the procedure used to fit the parameters in the model.

1. The volume of the nanorods V_p and the intensity I_0 at the trap focus were fitted from the measurement of the spectral intensity ratio (row a-f-k). Via eq. E.6 this spectral intensity ratio can be directly related to the rotational trap stiffness κ_r, in units of $k_B T$ (row b-g-l). Since the rotational trap stiffness is proportional to both the trap intensity and the rod volume ($Re\{\Delta\alpha\} \propto V_p$), the product of these two quantities can be fitted by matching the slope of the plot of κ_r versus trap power. The value for the intensity at the trap power can be fixed by demanding that the particle volume lies within the distribution of particle volumes measured from electron microscopy on the sample. Here, we still allow the volume of each of the three nanorods to be different, keeping the

average volume equal to the ensemble volume.

2. The effective temperature $\widetilde{T_B}$ for the orientation distribution can be found by fitting the observed curvature in the plot of κ_r versus trap power using a thermal energy that increases with trap power. Specifically, we evaluate the thermal energy as $k_B\widetilde{T_B} = k_B(T_0 + \widetilde{\Delta T_B})$, where T_0 is the bath temperature and the effective temperature increase $\widetilde{\Delta T_B}$ is proportional to the trap intensity. As the effective temperature increases, the plot of κ_r vs trap power becomes sublinear.

3. Step 1 and 2 are optimized recursively until satisfactory agreement is obtained. The values for the intensity of the trap I_0, the particle volume V_p and the effective temperature $\widetilde{T_B}$ are now fixed.

4. With the trap intensity and particle volume determined, the model is adjusted to the measured correlation times in row c-h-m. The rotation times are given as $\tau_r = \xi_r/(2\kappa_r)$. In the fit, we allow for an effective hydrodynamic volume V_{hyd} in the rotation friction coefficient ξ_r of the rod : $\xi_r = \widetilde{\eta}_r V_{\mathrm{hyd}} C_r$, with C_r a geometrical factor. The geometrical factor is taken as the one calculated for an ellipsoid (see Appendix D). In combination with the previously determined particle volume, the effective hydrodynamic volume determines the thickness of the capping layer. We adjust the hydrodynamic volumes of the three individual rod such that the thickness of the capping layer is the same for all three nanorods.

5. We find an effective rotational viscosity $\widetilde{\eta}_r$ as function of temperature by matching the observed curvature in the plot of rotation times versus trap power, using the known temperature dependence of the viscosity of water (Appendix D). Specifically, we evaluate the viscosity as $\widetilde{\eta}_r = \eta(T_0 + \widetilde{\Delta T_r})$, where η is the viscosity of water and the effective temperature increase $\widetilde{\Delta T_r}$ is proportional to the trap intensity.

6. Step 4 and 5 are optimized recursively until satisfactory agreement is obtained. The values for the hydrodynamic thickness and the effective rotational viscosity η_r are now fixed.

7. We fit the transverse trap stiffness κ_t from the measured translation correlation times τ_t (row d-i-n) using the relation $\tau_t = \xi_t/(2\kappa_t)$, where ξ_t is the friction coefficient for translations along the long axis of the rod. For the friction coefficient we use the value calculated for an ellipsoid

(Appendix D), taking into account the determined particle volume and the hydrodynamic thickness of the capping layer.

8. We find an effective translation viscosity η_t by matching the observed curvature in the plot of translation times versus power, using the known temperature dependence of the viscosity of water. Here we assume again that the increase of the particle temperature scales linearly with trapping power. However, in contrast to step 5, we evaluate the effective viscosities for translations as $\eta_t = \eta_{\text{HBM}}$, providing values for the effective temperature for Hot Brownian Motion T_{HBM} and the particle temperature T_p.

9. We interpret the values found for effective temperature $\widetilde{T_B}$ and effective viscosities $\widetilde{\eta}_r$ and $\widetilde{\eta}_t$ in terms of a corresponding particle temperature T_p. This particle temperature can be compared to a temperature calculated independently from the absorption cross section calculated for a gold nanorod with the fitted volume and measured aspect ratio, and the fitted trap intensity (see Appendix G).

The measurements on all three nanorods are well described by our model, when we take the effective viscosity for rotations $\widetilde{\eta}_r$ as the viscosity at the particle temperature, and the effective temperature $\widetilde{T_B}$ equal to the particle temperature. For simplicity, we have chosen to fit all three nanorods with the same hydrodynamic thickness of the PEG capping layer. The quality of the global fit could possibly be further improved by allowing for a variation of this parameter for the individual nanorods. This would be reasonable as the amount of PEG molecules may vary from rod to rod.